The Structure of Apo Human Glutamate Dehydrogenase Details Subunit Communication and Allostery

ARTICLE *in* JOURNAL OF MOLECULAR BIOLOGY · JUNE 2002

Impact Factor: 4.33 · DOI: 10.1016/S0022-2836(02)00161-4 · Source: PubMed

doi: 10.1016/S0022-2836(02)00161-4 available online at http://www.idealibrary.com on IDEAL® J. Mol. Biol. (2002) 318, 765–777

JMB

The Structure of Apo Human Glutamate Dehydrogenase Details Subunit Communication and Allostery

Thomas J. Smith[1]*, Timothy Schmidt[1], Jie Fang[2], Jane Wu[3] Gary Siuzdak[3] and Charles A. Stanley[2]

[1]*Donald Danforth Plant Science Center, 975 North Warson Road, St. Louis, MO 63132, USA*

[2]*Division of Endocrinology The Children's Hospital of Philadelphia, Philadelphia, PA 19104, USA*

[3]*The Scripps Research Institute Center for Mass Spectrometry and Department of Molecular Biology, BCC157, 10550 North Torrey Pines Road, La Jolla, CA 92037, USA*

**Corresponding author*

The structure of human glutamate dehydrogenase (GDH) has been determined in the absence of active site and regulatory ligands. Compared to the structures of bovine GDH that were complexed with coenzyme and substrate, the NAD binding domain is rotated away from the glutamate-binding domain. The electron density of this domain is more disordered the further it is from the pivot helix. Mass spectrometry results suggest that this is likely due to the apo form being more dynamic than the closed form. The antenna undergoes significant conformational changes as the catalytic cleft opens. The ascending helix in the antenna moves in a clockwise manner and the helix in the descending strand contracts in a manner akin to the relaxation of an extended spring. A number of spontaneous mutations in this antenna region cause the hyperinsulinism/hyperammonemia syndrome by decreasing GDH sensitivity to the inhibitor, GTP. Since these residues do not directly contact the bound GTP, the conformational changes in the antenna are apparently crucial to GTP inhibition. In the open conformation, the GTP binding site is distorted such that it can no longer bind GTP. In contrast, ADP binding benefits by the opening of the catalytic cleft since R463 on the pivot helix is pushed into contact distance with the β-phosphate of ADP. These results support the previous proposal that purines regulate GDH activity by altering the dynamics of the NAD binding domain. Finally, a possible structural mechanism for negative cooperativity is presented.

Keywords: human glutamate dehydrogenase; hyperinsulinism; allostery; subunit communication

Introduction

Mammalian glutamate dehydrogenase (GDH) catalyzes the reversible oxidative deamination of L-glutamate to 2-oxoglutarate using NAD(P)(H) as coenzyme. The enzyme is a homohexamer and each subunit has a molecular mass of ~56 KDa. The structures of several bovine glutamate dehydrogenase (boGDH) complexes have been determined.[1,2] Each subunit is composed of approximately three domains; the Glu binding domain at the N terminus, the NAD binding domain, and the antenna domain (Figure 1). The 48-residue antenna is not found in bacterial and fungal GDHs and was thought to be involved in allosteric regulation.[1,2]

The two major, opposing allosteric regulators, ADP and GTP, appear to exert their effects *via* abortive complexes (NAD(P)H·Glu and NAD(P)·αKG). ADP is an activator believed to act, at least in part, by destabilizing abortive complexes.[3,4] ADP also abrogates negative cooperativity.[5] In contrast, GTP is a potent GDH inhibitor and is thought to act by stabilizing abortive complexes.[6] GTP binding is antagonized by phosphate[7] and ADP,[8] but is synergistic with NADH bound in the non-catalytic site.[7] Finally, ADP and GTP bind in an antagonistic manner[8] where ADP and GTP bind preferentially to the open and closed states, respectively.[1,2] The GTP site lies between the NAD

Abbreviations used: GDH, glutamate dehydrogenase; boGDH, bovine GDH; HI/HA, hyperinsulinism/hyperammomemia.

E-mail address of the corresponding author: tsmith@danforthcenter.org

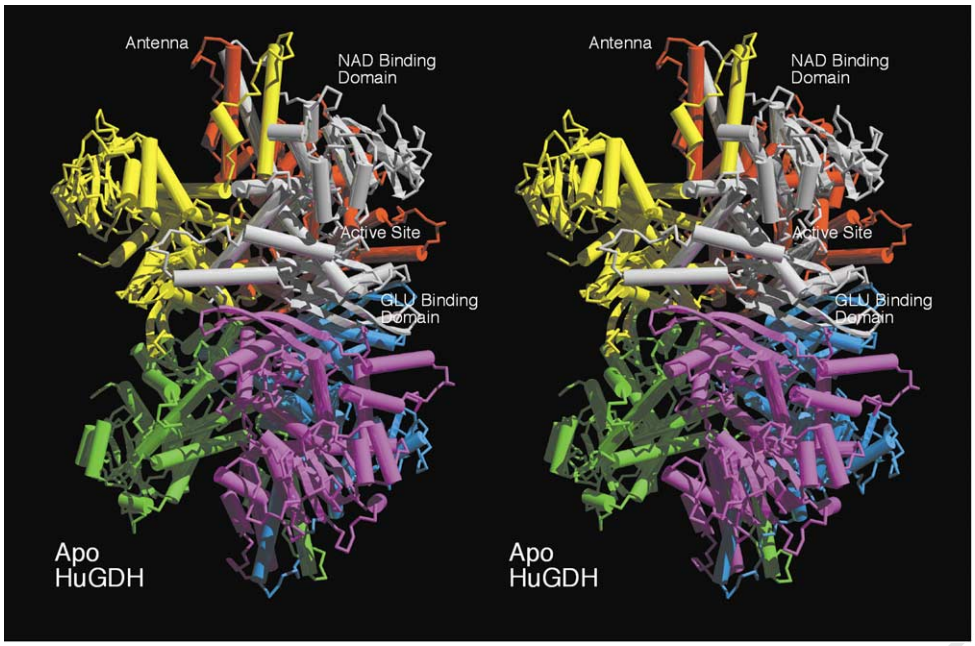

Figure 1. Ribbon diagram of the apo-huGDH structure. In this stereo image, the individual subunits are represented in different colors. The 3-fold axis runs vertically through the middle of the model. The antenna region is not found in bacterial or fungal GDH.

binding domain and the antenna[1,2] while the ADP site is under the pivot helix and behind the Glu binding domain.[2,9]

Bovine GDH has a second coenzyme site on each subunit that binds NAD(H) ~tenfold better than NADP(H)[10,11] with the reduced form binding better than the oxidized form.[12] It has been suggested that reduced coenzyme at this site inhibits the reaction[10,11] while oxidized coenzyme binding causes activation.[13] Recent studies on several boGDH complexes have shown that NAD(H), but not NADP(H), binds to the putative ADP site.[2] These studies also suggested that NADH inhibition might not be due to NADH binding to this site. Both coenzymes (i.e. NADP(H) and NAD(H)) exhibit strong negatively cooperative binding in the presence of substrate in mammalian GDH.[14,15]

While this enzyme has been extensively studied over the past five decades, several fundamental issues remain. Firstly, the catalytic direction *in vivo* remains highly controversial. Secondly, since there are many pathways that can synthesize glutamate and 2-oxoglutarate independent of GDH, it is unclear as to why mammals produce such large amounts of this mitochondrial enzyme. Finally, only GDH from higher organisms is allosterically regulated, but the reason for this is unknown.

Clues as to the physiological roles of GDH and its allosteric regulation have recently been revealed by the finding that the hyperinsulinism/hyperammonemia (HI/HA) syndrome in humans is caused by defects in GDH regulation.[16,17] These patients are heterozygous for mutant forms of GDH that are unresponsive to the inhibitor, GTP. The results from these studies suggested that GDH mainly operates in the oxidative deamination reaction in the pancreas and liver, and may be involved in insulin homeostasis.

Presented here is the structure of human glutamate dehydrogenase (huGDH) that was crystallized in the absence of allosteric or active site ligands and also studied in solution using protein mass mapping.[18–24] In this apo form, the GTP binding site is distorted such that it is unlikely that GTP can bind to the enzyme in this open conformation. In contrast, the adenosine–ribose pocket in the putative ADP binding site remains unchanged as the catalytic cleft opens and it is likely that R463 forms a salt-bridge with the β-phosphate of ADP. Structural changes were found in the descending strand helix that may account for how subunits communicate during negative cooperativity. Finally, a number of HI/HA mutations are found in this section of the antenna domain but none of these residues contact GTP. Therefore, this subset of HI/HA mutations may abrogate GTP inhibition *via* interference with antenna-associated subunit communication.

Results

Domain movement

Since HuGDH and boGDH share at least a 96% sequence identity, it was not surprising that most of the domain structures of these two enzymes are identical (Figure 1). Unlike boGDH complexed with active site ligands, the catalytic cleft of apo huGDH is in the open conformation (Figures 1, 2, and 4). A number of areas of this huGDH structure are very disordered. The *B* values in the final

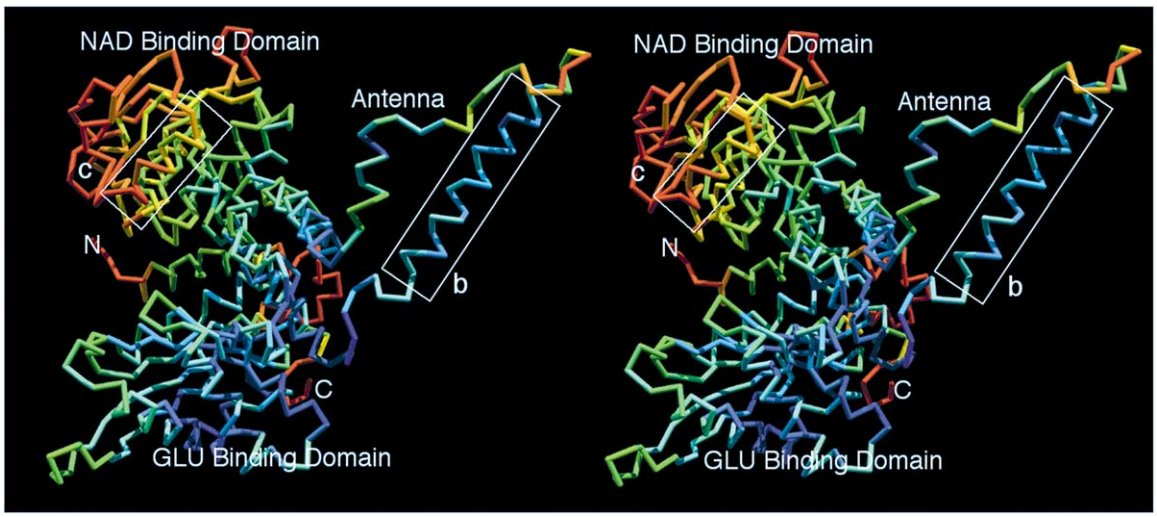

Figure 2. *B*-value distribution in apo huGDH. Stereo view of the C^{α} backbone of one subunit of huGDH colorized according to *B*-values. The *B*-values ranged from 2 Å^2 (blue) to 100 Å^2 (red). In this orientation, the 3-fold axis lies approximately vertically along the right side of the Figure. The 2-fold related subunit lies horizontally towards the bottom of the Figure. The most disordered regions are at the upper left portions of the NAD binding domain and the α1–α2 loop at the back of the Glu binding domain. The white boxes outline the regions that have typical (b; Figure 3(a)) and poor (c; Figure 3(b) and (c)) electron density.

model ranged from 2 to 100 Å^2 with an average *B* value of 54 Å^2. As shown in Figures 2 and 3, the two most disordered regions were at the top of the NAD binding domain furthest from the pivot helix and the first loop at the back of the glutamate-binding domain connecting the α1 and α2 helices. While the density elsewhere in the model allowed for unambiguous interpretation (Figure 3(a)), the model in these areas was built by placing large sections of the secondary structure from the boGDH model into the diffuse density (Figure 3(b) and (c)). As shown in Figure 4, these disordered regions were on the portions of the atomic structure that undergo the greatest displacement when the catalytic cleft opens. It was possible that this apparent disorder was due to different NAD binding domain orientations amongst the six subunits. To test for this possibility, each of the six subunits was divided into five domains roughly corresponding to the glutamate-binding domain, the NAD binding domain, the antenna, the pivot helix, and the α-helix at the C terminus. This segmented model was subjected to rigid body refinement and then full refinement using X-PLOR. This protocol greatly improved the refinement statistics. While all segments could have shifted during this procedure, only the NAD binding domain orientation, relative to the Glu binding domain, differs amongst the six subunits. Compared to the first subunit, these deviations yielded displacements of 3.9, 4.1, 1.1, 1.3, and 2.0 Å at the outermost portions of the NAD binding domain. While this protocol improved the refinement and electron density for these regions (Figure 3(b) and (c)), the *B*-values still get progressively worse with increasing distance from the pivot helix (Figure 2). Therefore, it is clear that each of the NAD binding domains are in unique orientations and it appears that they are more mobile than most of the rest of the structure.

The six glutamate-binding domains form the core of the GDH hexamer. The conformation of this central region does not change as the catalytic mouth opens. Therefore, to illustrate the conformational changes that occur as the NAD binding domain moves, the glutamate binding domains of the apo huGDH and complexed boGDH were aligned as shown in Figure 4. The transition from closed to open conformation starts with the movement of the NAD binding domain away from the Glu binding domain by ~18°. In the previous modeling exercise, the opening of the catalytic cleft was simulated by rotating the NAD domain about the long axis of the "pivot helix". While this general motion does indeed occur (Figure 4, movement 1, 2), the entire NAD binding domain also twists about the antenna in a clockwise direction. This rotation is associated with a concomitant clockwise twist in the ascending antenna helix (Figure 4, movement 3). As the helix and the NAD binding domain twist, the tip of the antenna becomes mostly disordered and the helix on the descending strand increases in length (Figure 4, movement 4). In a manner not fully modeled in the previous studies,[2] the α1 and α2 helices appear to be associated with the NAD binding domain and undergo very large conformational changes. The α1 helix appears to rotate about its center of mass with the N terminus rotating up with the NAD binding domain (Figure 4, movement 5). This motion forces the α2 helix down in a clockwise direction (Figure 4, movement 6). All of these conformational changes are absorbed before the beginning of the first β-strand of the glutamate-binding domain that remains fixed during these

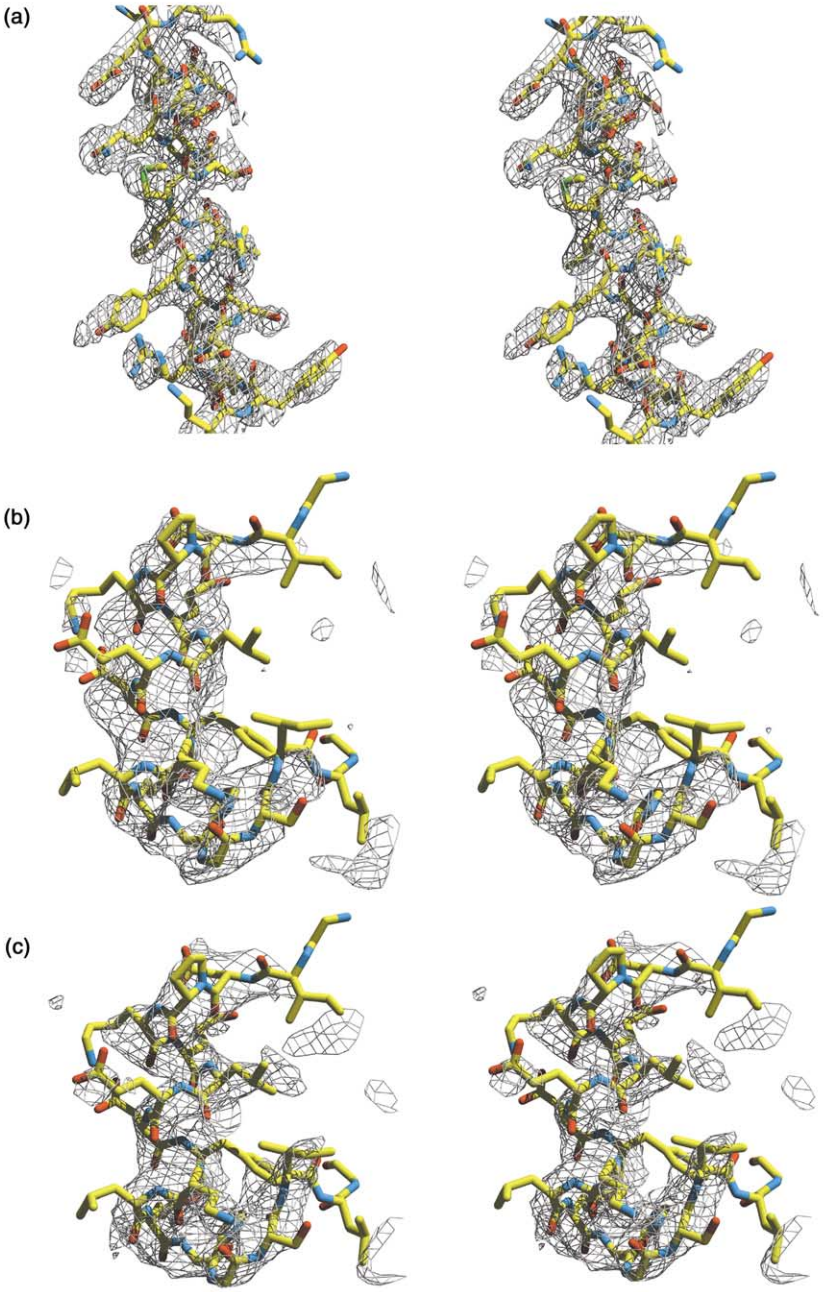

Figure 3. Example electron density in huGDH. (a) Electron density and model of the ascending α helix in the antenna domain. The density shown here was 6-fold averaged using a single mask and the program RAVE. In this Figure, the oxygen, nitrogen, and carbon atoms are colored red, blue, and yellow, respectively. The electron density in this region, shown as a gray cage, is typical of much of the Glu binding, pivot helix, and antenna domains. (b) Example of electron density in the poorly ordered regions. The density shown here was 6-fold averaged for ten cycles using a single mask and the program RAVE. (c) In contrast to (b), the electron density shown here was generated using a separate mask for the NAD binding domain. Note the marked improvement and, hence, the justification of using multiple domains for structure refinement.

movements. The density around the α1–α2 turn is much weaker than in the "closed mouth" conformation, suggesting that this region is more flexible in the apo form.

What is particularly interesting is the change in the helix in the descending strand of the antenna (Figure 4, movement 4). It is important to note that the electron density in this region is well defined in both the apo and complex forms of the enzyme. As the mouth opens, this region appears to "recoil" in a manner akin to an extended spring regaining its shape. This is made evident by the fact that the hydrogen-bonding pattern is greatly improved (Figure 5(a) and (b)) and the psi–phi values of this helix in apo-GDH cluster more tightly in the helical region of the Ramachandran plot (Figure 5(c) and (d)). As shown in Figure 5, G446 moves into a helical conformation as the mouth opens. Interestingly, this is a region in which a number of HI/HA mutations are found (noted with asterisks in Figure 5(a) and (b) and boxes in Figure 5(c) and (d)), yet none of these residues contact the bound GTP.

Conformational flexibility

To examine further the dynamic nature of mammalian GDH, limited proteolysis was performed on boGDH in the presence of various ligands and the resulting protein fragments were analyzed using mass spectrometry (Figure 6, Table 1). In the absence of ligands, a major peak appears within

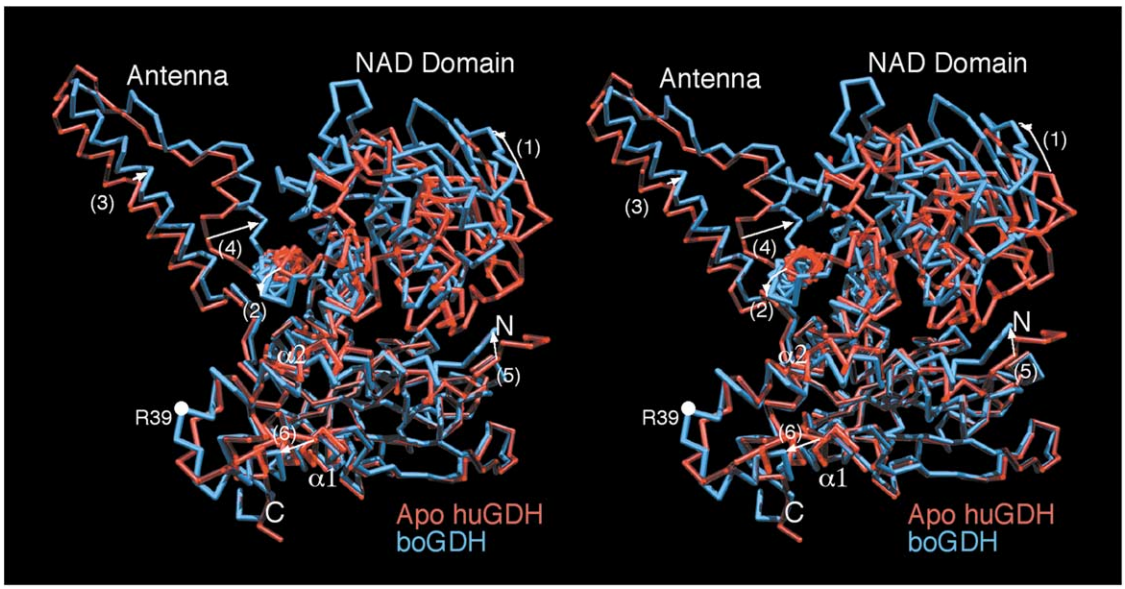

Figure 4. Comparison between the open and closed conformations of mammalian GDH. Shown in this Figure are single subunits of the boGDH·NADH·Glu·GTP complex in the closed mouth conformation (translucent red) and the apo huGDH structure in the open mouth conformation (blue). The orientation in this Figure is with the 3-fold axis lying approximately vertically along the left side of the Figure, and the nearest 2-fold axis lying horizontally along the bottom of the Figure. The major site of trypsin cleavage is highlighted by the white ball at R39. The general domain motions are highlighted by the white arrows.

minutes corresponding to cleavage at R39 that lies on the loop between α1 and α2 (Figure 4). This peak was therefore used to monitor proteolytic sensitivity.

From these results it is apparent that only active site ligands can protect this loop from being cleaved by trypsin. The complexes that best abrogate cleavage are the NAD(P)H·Glu·GTP and the NAD(P)H·Glu (samples 3, 4, 6, and 8). This protective effect is unlikely due to coenzyme binding to the regulatory site since NADPH, which does not significantly bind to this site under these conditions, protects the enzyme nearly as well as NADH. GTP alone does not afford much protection against tryptic digestion (sample 5). NADH and glutamate alone are able to abrogate proteolysis to some degree (samples 9 and 10, respectively). These results suggest that the closed mouth conformation exhibits less conformational dynamics than the open mouth conformation. Abortive complexes bind more tightly to the enzyme than coenzyme or substrate alone. This correlates well with the ability of these combinations of ligands to protect the R39 site better than either ligand alone. Interestingly, the structure of the binary complex of csGDH has been determined and the catalytic mouth is not closed as tightly as that observed in the boGDH ternary complexes.[25,26] Therefore, these mass spectrometry results are consistent with the observation that the electron density of the α1–α2 turn becomes disordered in the apo structure and suggests that the NAD binding domain is highly mobile in the absence of active site ligands.

Conformational changes in the GTP site

In the previous modeling exercise, it was assumed that the pivot helix moves with the NAD binding domain and that together they rotate about the long axis of the helix.[2] However, as shown in Figure 7(a), it is apparent that the NAD binding domain actually twists about the pivot helix. For these analyses, the open and closed conformations were aligned according to the pivot helix. The GTP molecule shown in Figure 7 is from the "closed conformation" of the boGDH·NADH·Glu·GTP complex. It is clear from Figure 7(a) that this motion of the NAD binding domain relative to the pivot helix directly affects the GTP site. Some of the residues that contact the bound GTP molecule in the boGDH·NADH·Glu·GTP complex are further detailed in Figure 7(b). Residues that were found to be mutated in the HI/HA syndrome are noted with asterisks. H454 and H213 lie on the pivot helix and therefore their C^{α} positions do not move appreciably during to the alignment procedure. R265 normally stacks against the purine ring and interacts with the γ-phosphate of the bound GTP. However, in this open conformation, the stacking interaction is gone and the side-chain is now too close to the γ-phosphate. In the closed conformation, R269 and R221 made extensive interactions with the γ-phosphate but are now too far away to interact in the open conformation. Interestingly, this movement about the pivot helix moves the floor of the GTP binding pocket (I216 and S217) up towards the GTP molecule, thereby sterically blocking GTP binding.

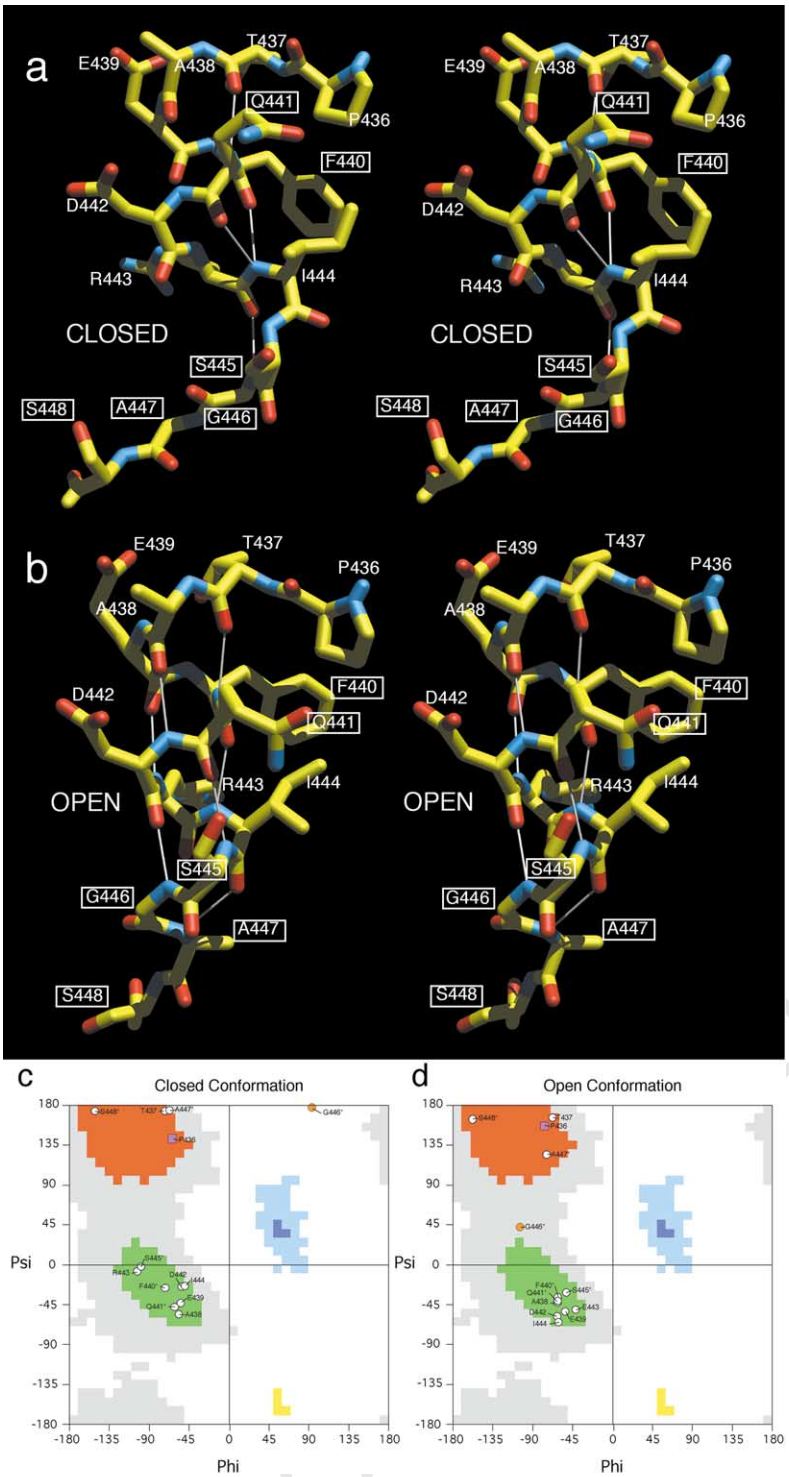

Figure 5. Changes in the conformation helix in the descending strand of the antenna. Shown here is the conformational change in the antenna as the catalytic mouth moves from the closed (a) to the open (b) conformation. The carbon, nitrogen, and oxygen atoms are colored yellow, blue, and red, respectively. The residues that were found to mutate in the HI/HA syndrome are encircled by white boxes. Possible hydrogen bonds (N and O atoms within a distance of 2.8 to 3.2 Å) are highlighted by thin white tubes. Shown in (c) and (d) are the Ramachandran plots of the same helical region in the closed and open forms, respectively. The β-strand, α-helical, and β-turn regions are highlighted in red, green, and blue, respectively. The residues are labeled, with the proline residues represented by mauve squares, glycine residues by orange spheres, and all others by white spheres.

Therefore, it is quite apparent that GTP cannot bind to GDH until the catalytic cleft closes. This is consistent with the mass spectrometry results that suggested that GTP did not affect the dynamic nature of apo boGDH and that there is binding synergism between the abortive complex and GTP.

Conformational changes in the ADP site

In the previous modeling exercise, it was hypothesized that the pivot helix would rotate about the long axis and this movement would place R463 into contact with the β-phosphate of ADP. As shown in Figure 8, this general motion does indeed occur. For this analysis, the glutamate binding domains of the apo and complex forms were aligned. The ADP molecule shown in this Figure is derived from the second bound NADH molecule observed in the boGDH·NADH·Glu·GTP complex.[2] In this complex, the NADH molecule adopted two different conformations: one where the nicotinamide/ribose moiety pointed up

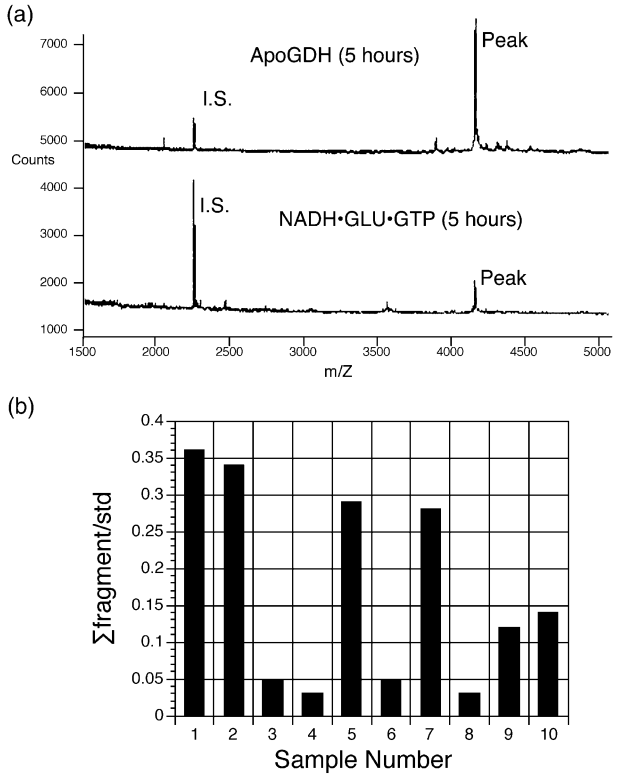

Figure 6. MALDI-MS analysis of limited trypsin digestion of boGDH in the presence of various allosteric and active site ligands. (a) MALDI analysis of boGDH in the absence of ligands (top) and in the presence of the NADH, Glu, and GTP (bottom). The major peak downstream from the internal standard (I.S.) corresponds to the 1–39 fragment and was used to monitor digestion. (b) Integrated area of the 1–39 fragment peak compared to the internal standard. The key to the sample number is shown in Table 1. Note that the best protection of this cleavage is afforded by active site ligands even though the cleavage site is distal to the active site.

towards the pivot helix and one where it pointed down towards the intra-trimer subunit interface.[2] The adenosine, ribose, and α-phosphate positions were the same in both conformations. For the β-phosphate shown in this model, the "up" conformation was used since it made more contacts with the surrounding protein. As shown in this Figure, the contacts between ADP and GDH are mainly mediated by the purine–ribose moieties. This binding pocket does not change upon the opening of the active site. The pivot helix draws closer to the bound ADP by virtue of the clockwise rotation about the antenna and moves R463 into salt-bridging contact with the β-phosphate of the bound ADP. This is entirely consistent with the previous result demonstrating that a R463A mutation abrogates ADP activation.[9]

Possible subunit communication

Since the six glutamate binding domains form an apparently rigid core structure as the catalytic cleft opens and closes, it seems likely that the subunit communication responsible for negative cooperativity occurs *via* intra-trimer contacts. Bacterial GDH does not exhibit negative cooperativity and does not have the antenna domain. Therefore, it was concluded that the antenna might play a major role in subunit communication.[1,2] To examine further the changes in the intra-trimer contacts, two of three trimeric subunits were aligned *via* the ascending helices of the antenna in the A subunits (Figure 9).

During negative cooperative binding of coenzyme, the binding (and subsequent cleft closure) occurs more facilely in the first subunit than in subsequent subunits. What is not clear is how this apparent asymmetric binding is imposed in this symmetrical oligomer. It is clear that if one subunit closes upon substrate and coenzyme, the intra-trimer interface is greatly altered. As shown in Figure 9, as one subunit (green) closes, the NAD binding domain twists in a counter-clockwise direction (arrow 1) and results in a number of contortions in the helix. Perhaps most importantly, closure of this subunit requires the small helix on the descending strand to become distorted and it is pushed into the antenna of the adjacent subunit (arrow 2). This movement also pushes the tip of the antenna up (arrow 3). However, this latter motion may not require much energy since this region is very disordered in the apo structure. In order for the adjacent subunit to close, it needs to twist the antenna in a counter-clockwise manner. It may be that the changes in the descending strand of the first subunit make this transformation energetically unfavorable in adjacent subunits. It is interesting to note that ADP abrogates negative cooperativity and binds in the center of these conformational changes.

Table 1. Ligands added during MALDI-digestion experiments

Sample	[Glu] (mM)	[NAD(P)H] (mM)	[GTP] (mM)	[ADP] (mM)
1	0	0	0	0
2	0	0	0	2.0
3	20	1.5 NADH	1.5	0
4	20	1.5 NADPH	1.5	0
5	0	0	1.5	0
6	20	1.5 NADPH	0	0
7	0	1.5 NADPH	0	0
8	20	1.5 NADH	0	0
9	0	1.5 NADH	0	0
10	20	0	0	0

Hyperinsulinism/hyperammonemia mutations

Most of the HI/HA mutations are at residues that make direct contact with the inhibitor GTP.[1,2] However, a number of the HI/HA mutation sites lie on the descending strand of the antenna that do not contact the bound GTP. These latter antenna mutations are summarized in Table 2. All of these residues contact the adjacent subunit within the

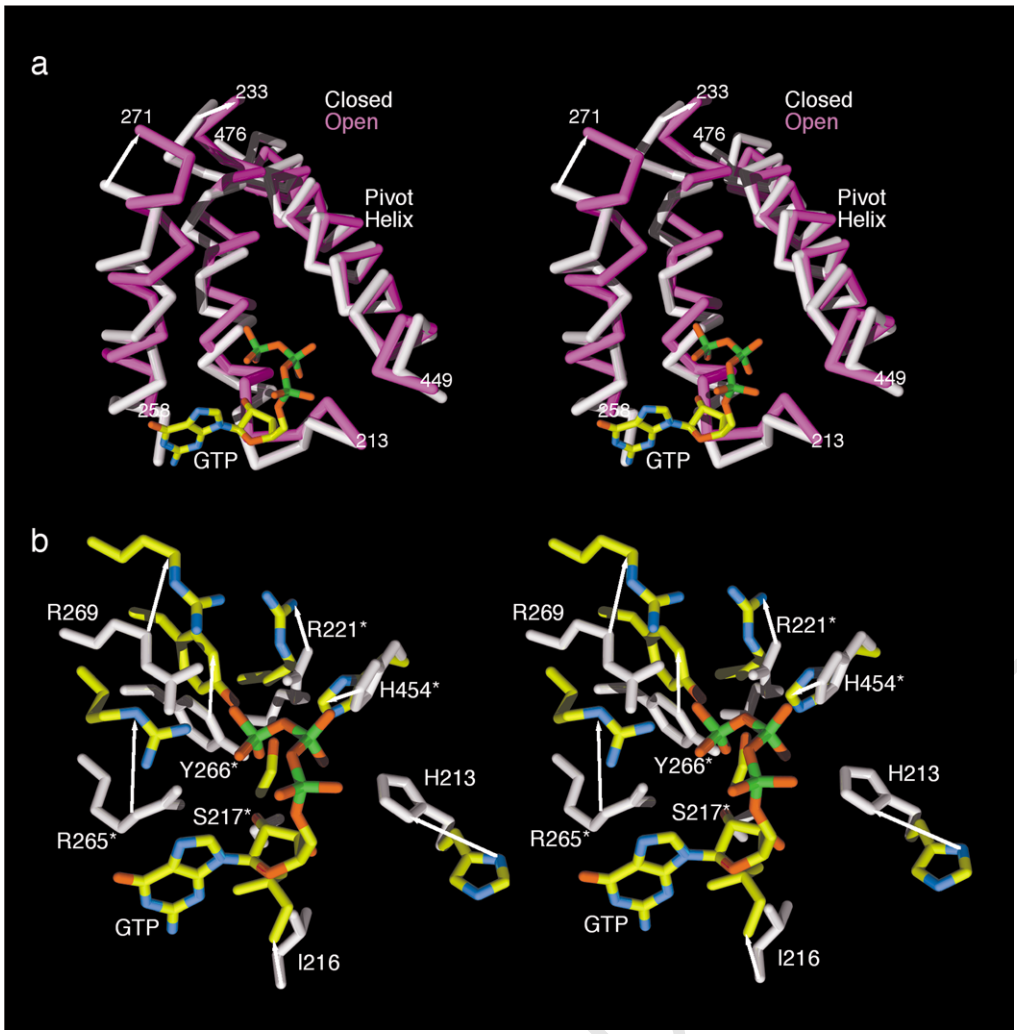

Figure 7. Changes in the GTP site as the catalytic mouth opens. Shown here are three helices around the GTP binding site in the open (mauve) and closed (white) conformations. For this analysis, the two NAD binding domains are aligned according to the pivot helix. The bound GTP molecule from the boGDH·NADH·Glu·GTP complex is also shown using the same color code as the other Figures with the exception that the phosphate molecules are colored green. In this view, the antenna is on the right, and the catalytic mouth is towards the bottom. (b) A detailed view of the changes in the GTP binding site as the catalytic mouth opens. Here, the side-chains of the closed conformations colored in white and the open form side-chains are colored by atom type. The arrows denote motion as the catalytic mouth opens. The mutation sites that cause the HI/HA syndrome are denoted by asterisks. As above, the two NAD binding domains were aligned according to the pivot helix and the orientation is the same as in (a).

trimer. N410 and L413 lie on the ascending helix of the antenna that undergoes the counter-clockwise twist as the catalytic mouth opens. The remaining residues lie in the helix of the descending strand that lengthens as the catalytic mouth opens (Figure 5). Of these mutations, most lie in the portion of the strand that undergoes the greatest conformational changes. In particular, a number of mutations lie at G446. Clearly, the loss of flexibility in this residue will have a deleterious effect on the ability of the antenna to undergo the required conformational changes. According to various secondary structure prediction programs such as SSP,[27] nearly all of these mutations are predicted to stabilize the helix. If this is indeed the case, then many of these HI/HA mutations may stabilize the open mouth conformation. This also suggests that somehow GTP inhibition requires facile antenna deformation as the mouth closes.

Discussion

As has been observed in bacterial glutamate dehydrogenase, the NAD-binding domain clamps down upon the glutamate-binding domain as substrate and coenzyme bind in the catalytic cleft. It is clear that, in the absence of active site ligands, the "open mouth" conformation is preferred. In this state, the NAD binding domain and the α1–α2 loop are relatively mobile with the latter region being particularly sensitive to trypsinolysis. This

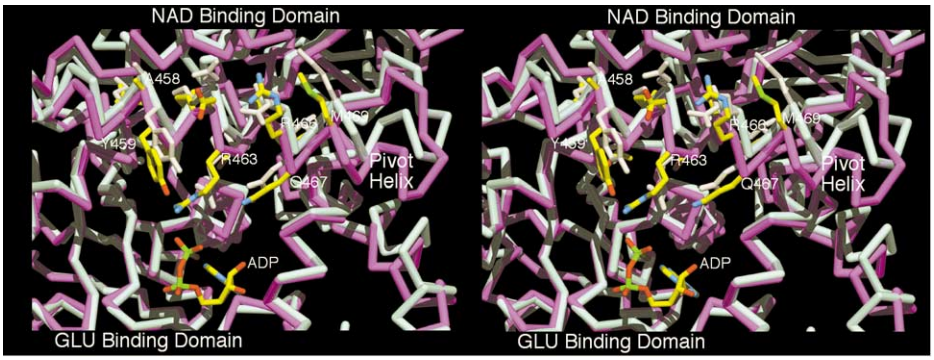

Figure 8. Changes in the putative ADP binding pocket upon opening of the catalytic cleft. Shown in this Figure are the changes in the binding environment of ADP. For this analysis, the Glu binding domain of the closed mouth form of boGDH (pale blue) was aligned to that of the apo huGDH structure (mauve). The ADP molecule shown in this Figure is derived from the second NADH molecule found in the boGDH·Glu·NADH·GTP structure but with the nicotinamide–ribose moiety removed. The side-chains of the nearby pivot helix residues of the huGDH structure are colored according to the atom type while those of the boGDH structure are shown in white. Note how the movement of the pivot helix brings R463 and Q467 into close proximity to the β-phosphate of the bound ADP while the conformation of the adenosine–ribose binding pocket remains relatively unchanged. This is consistent with the previous finding that an R463A mutation abrogates ADP activation.

implies that before substrate and coenzyme bind, the NAD binding domain is sampling several different conformations. Upon substrate and coenzyme binding, the additional energy drives the catalytic mouth shut into a more rigid conformation. Perhaps most importantly, the α-helix in the descending strand is longer with better geometry in the apo state than in the closed state. From the location of several HI/HA mutations, and their predicted effects on this helix, it appears that GTP inhibition is at least partially dependent on the ability of this helix to distort as the mouth closes.

It is possible that the previous abortive complex structures represent a "hyper-closed" mouth conformation. Substrate and coenzyme bind tighter in the abortive complex than in the normal ternary complex. This is consistent with the finding that the catalytic cleft of these abortive complexes is more tightly closed than in the bacterial binary complexes.[1] Such hyper-closure might make the GTP binding site more available to GTP and therefore explain the synergism between the GTP binding site and the active site. Furthermore, it is possible the subset of HI/HA mutations in the helix of the descending strand stabilize this helical

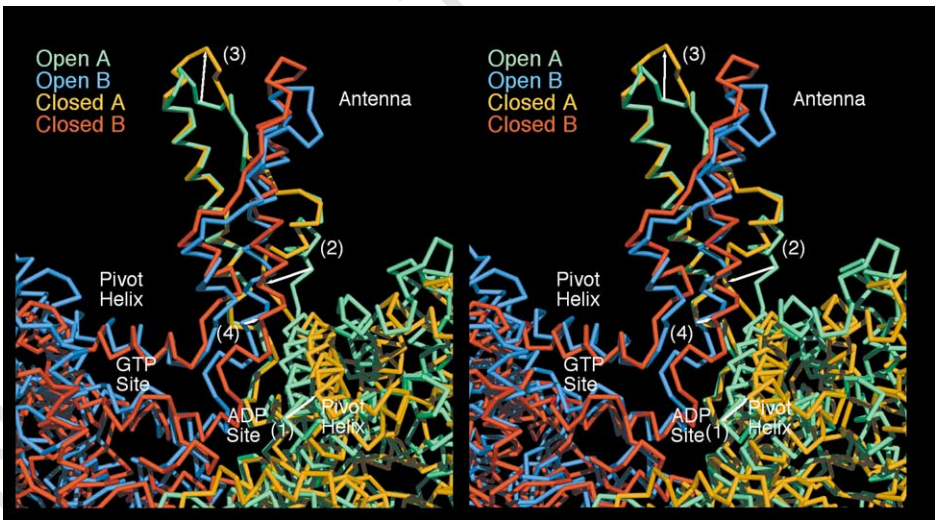

Figure 9. Possible mechanism of antenna-mediated negative cooperativity. Shown in this Figure are two adjacent subunits of the huGDH model (green and blue) aligned by one of the ascending antenna helices of the closed boGDH model (orange and red). The 3-fold axis runs vertically through the middle of the Figure and the third subunit of this trimer has been eliminated for clarity. The arrows indicate the conformational changes that occur as the first subunit closes down upon the substrate and coenzyme. Note how the helix in the descending strand (movement 2) becomes distorted and forced into the core of the antenna as the catalytic cleft closes.

Table 2. HI/HA mutations that lie in the antenna domain

Residue	HI/HA mutation
N410	T, Y
L413	V
F440	L
Q441	R
S445	L
G446	R, D, C, S, V
A447	T
S448	P

region, thereby inhibiting hyper-closure. This would be expected to have a deleterious effect on GTP binding and inhibition. Alternatively, it may be that these HI/HA mutations affect intra-trimer communication that may be mediated by these changes in the antenna and required for GTP inhibition. Evidence of such communication is found in that the heterotrimeric GDH made by the HI/HA patients appears to exhibition a monophasic rather than a biphasic response to GTP.[9] These results suggest that the effects of the mutations, and therefore the process of GTP inhibition as well, are not isolated to individual subunits.

These results are consistent with the previously proposed model where GTP and ADP act by controlling the dynamics of the NAD binding domain.[2] While many allosteric enzymes are often described as existing in an inhibited (T) or activated (R) state, this is not appropriate in the case of GDH. During catalysis, GDH needs to cycle between the open and closed positions. Locking the enzyme into one particular state will prevent enzymatic turnover. The ADP site is available in either the open or closed state. However, in the open state, R463 is rotated about the antenna and pivot axes such that it interacts with the β-phosphate of ADP. Such interaction may not lock the enzyme into a particular conformation but rather facilitate the opening of the catalytic cleft. Since ADP has been shown to eliminate the formation of abortive complexes,[5] perhaps this interaction prevents hyper-closure of the catalytic cleft. In contrast, GTP cannot bind to the apo state of the enzyme. Once coenzyme and substrate are bound, GTP binds and increases the apparent affinity by preventing the opening of the catalytic cleft. In this way, GTP and ADP bind antagonistically to the enzyme since they have opposite effects on NAD binding domain dynamics.

The large conformational change that occurs in the antenna as the catalytic site opens and closes may play a role in negative cooperativity. Since the only structures determined to date have all subunits in one conformation or another, one can only surmise as to how closure of one subunit will affect adjacent subunits. It may be that as a subunit closes, the helix on the descending strand distorts and moves towards the clockwise-related subunit. These new contacts may make it more difficult for the adjacent subunit to close its catalytic cleft, thereby causing negative cooperativity.

The structural changes in the antenna may explain how negative cooperativity is exerted, but does not explain why it occurs. There are at least three reasons why GDH might exhibit negative cooperativity:

(a) Negative cooperativity may be used by the enzyme to insure a constant catalytic turnover over a wide range of coenzyme concentrations. Higher concentrations of coenzyme decrease binding constants and cause attenuated activity. However, it is not clear that coenzyme concentrations in the mitochondria vary enough to require such attenuation.

(b) Negative cooperativity may be used by the enzyme to facilitate catalytic turnover *via* a reciprocating subunit mechanism.[28,29] This model is similar to the ATPase mechanism where the energy of product binding is transferred mechanically to adjacent subunits to facilitate product release. The structural changes observed in the antenna give one possible mechanism as to how this mechanical energy might be transferred from one subunit to the next. However, it would follow that the mammalian enzyme is more efficient than the bacterial form. It is not apparent that the mammalian form is more efficient than the bacterial form, nor is it clear why mammalian GDH would need to be more efficient.

(c) Negative cooperativity may be a consequence of the subunit communication needed to facilitate heterotrophic allosteric regulation. This enzyme acts like a motor with the NAD binding domain rotating up and down during catalytic turnover with GTP and ADP affecting the movement of this domain. From the results on the HI/HA mutations, it appears that the effects of these regulators are not limited to the subunits to which they are bound. Therefore, extensive subunit communication may exist to facilitate purine regulation but result in negative cooperativity.

From the work on the HI/HA syndrome, it is apparent that mammalian GDH plays a crucial role in insulin homeostasis. As mammalian GDH evolved from more primitive organisms, ADP and GTP regulation was added. This regulation may make GDH an energy sensor to help control insulin secretion in the pancreas. From these results, the antenna domain appears to play a significant role in this process.

Materials and Methods

HuGDH expression

A full-length human GDH cDNA/pcDNA3 construct was made as previously described.[9] HuGDH was co-expressed with the chaperone proteins, GroES and

GroEL, using pGroESL.[9] The transformed bacteria were grown in 15 l of LB broth at 37 °C to A_{600nm} 0.6, and induced with 0.5 mM of isopropyl-β-D-thiogalactoside (IPTG) at 23 °C for 20 hours. The cells were pelleted at 8000*g*, and resuspended in GDH buffer (10 mM $NaKHPO_4$ (pH 7.4), 1 mM EDTA) with added 5 mM DTT and Protease Inhibitor Cocktail Tablets (Boehringer, Mannheim). Cells were lysed by sonication and solubilized by adding 1% (v/v) Triton X-100.

Purification of expressed huGDH

The supernatant from 15 l of culture was bound onto Q Sepharose Fast Flow anion exchange column (Amersham-Pharmacia Biotech) with a bed volume of 100 ml, washed with eight liters of GDH buffer until the A_{280nm} was <0.1, and then eluted with one liter (total elution volume) of a linear NaCl gradient (20 mM to 250 mM in GDH buffer). Positive fractions were combined, $(NH_4)_2SO_4$ was added to a final concentration of 1.4 M, and then loaded onto an omega-aminopentyl hydrophobic interaction column (Sigma) with a bed volume 100 ml, and washed with three liters of 1.4 M $(NH_4)_2SO_4$ in GDH buffer until the A_{280nm} was <0.1. GDH was eluted with 1.2 l (total elution volume) of a linear gradient of $(NH_4)_2SO_4$ (1.4 M to 0.7 M in GDH buffer). Positive fractions were pooled, concentrated, and desalted. The resulting GDH was bound to 5 ml of GTP-agarose affinity resin (Sigma) and washed with vacuum filtration. The resin-bound GDH was washed ten times with 50 ml GDH buffer and eluted with 25 ml 200 mM NaCl in GDH buffer at 4 °C for five minutes. The GDH fractions were pooled, desalted, and stored in 60% $(NH_4)_2SO_4$ at 4 °C. The final yield of GDH activity was 23% and ~12 mg/15 l. Purified GDH protein concentrations were determined by absorption at 280 nm based on an extinction coefficient of 0.93 cm^2/mg. Bacterial GDH does not bind to the GTP affinity column, as made evident by SDS-PAGE analysis, and therefore did not pose a problem during purification.

Crystallization and data collection

HuGDH was crystallized using the vapor diffusion method and sitting drop apparatus. The reservoir solution contained 1% (w/v) octyl-β-glucopyranoside, 1 mM sodium azide, 50 mM sodium chloride, 8% (v/v) methyl pentanediol, 0.1 M sodium phosphate (pH 7.3). The solution of enzyme contained 18 mg/ml enzyme in 0.1 M sodium phosphate buffer (pH 7.0). The sitting drop was composed of 1.1 μl water, 7.0 μl reservoir solution, and 1.9 μl of the huGDH solution. Crystals formed within two to three weeks. For data collection, a crystal was chosen with dimensions of 0.3 mm along two dimensions and 0.13 mm along the third. This crystal was frozen in a liquid nitrogen stream using the Oxford cryosystem. To prepare for freezing, the crystal was transferred to solutions that contained increasing concentrations of glycerol: 0, 2, 5, 10, 12.5, 15, 17.6, and 20%. The buffer used for these transfers contained 0.1 M sodium phosphate buffer (pH 7.1), 1% octyl-β-glucopyranoside, 0.08% methylpentanediol, 50 mM sodium chloride, and 0.1 mM sodium azide. The crystal was incubated for 20–30 minutes in each solution.

Data were collected using an R-Axis IV system attached to a Rigaku X-ray generator. The crystal to film distance was 250 mm and the oscillation angle was 0.8°. An exposure time of 30 minutes was used for each frame and 170° of reciprocal space was collected. The Bragg intensities were integrated with the program DENZO[31] and scaled using the program, SCALEPACK.[32] The crystal belongs to the triclinic space group with unit cell dimensions of $a = 97.8$ Å, $b = 98.8$ Å, $c = 124.2$ Å, $\alpha = 86.26°$, $\beta = 70.28°$, and $\gamma = 60.34°$. The redundancy for the data between 8 and 2.7 Å was 2.1. A summary of the data statistics is shown in Table 3.

Table 3. Data statistics

Resolution	R_{sym}	%Total	No. reflections	I/σ
30.00–5.39	0.042	98.2	12,855	24.4
5.39–4.28	0.049	97.8	12,731	21.2
4.28–3.74	0.054	97.7	12,803	15.9
3.74–3.40	0.068	97.3	12,703	10.0
3.40–3.16	0.097	97.0	12,674	6.0
3.16–2.97	0.128	96.6	12,616	4.1
2.97–2.82	0.170	84.4	11,019	3.0
2.82–2.70	0.216	54.8	7168	2.2
Total	0.047	90.5	94,574	14.8

Structure determination

The structure was determined using the molecular replacement method. From the cell dimensions and the self-rotation function calculations, it was most likely that there was a single hexamer in the triclinic cell. For subsequent cross-rotation function searches, a "mock open" model from previous boGDH studies was used.[2] This model was created by aligning the NAD and glutamate binding domains onto those of the apo *Clostridium symbiosum* structure.[33] Using the program X-PLOR,[34] the highest rotation function value was ~20% greater than that of the next cluster. The mock apo model was rotated to the appropriate orientation and subjected to rigid body refinement in X-PLOR. The entire hexamer orientation was refined and then each of the six subunits were divided into five smaller domains and each domain was independently subjected to rigid body refinement; 1–208, 209–390, 391–445, 446–475, and 476–501 (boGDH numbering). These domains roughly correspond to the glutamate-binding domain, the NAD binding domain, the antenna, the pivot helix, and the descending helix at the carboxyl terminus, respectively. The subunits were divided into these domains since it seemed likely that the mock model was not entirely accurate and it was also possible that subunits of this negatively cooperative enzyme might not all have identical conformations. The initial *R*-factor was 50%, which dropped to 47% after rigid body refinement, and then to 32% after ~60 cycles of energy minimization.

Upon examination of the model, it was initially apparent that there were statistically insignificant structural differences among the six subunits and therefore the electron density was 6-fold averaged using a single mask and the program RAVE. The final averaging statistics are shown in Table 4. While the outer regions of the NAD binding domain and first turn at the N terminus were disordered, the majority of the remaining electron density was easily interpreted. The model was then rebuilt using the program O and refined further with X-PLOR. For subsequent refinement, the subunits were divided into the same five domains used for rigid body refinement and each domain was restrained amongst the six subunits. Using 5% of the reflections,

Table 4. Refinement statistics

Refinement resolution range (Å)	8–2.7
I/σ cutoff	2.0
6-Fold averaging (%)	
C.C.	91.2
R-factor	25.8
RMS bond error (Å)	0.008
RMS angular error (°)	2.1
Model R_{work} (%)	26.3
Model R_{free} (%)	30.2
Ramachandran	
% Favored	85.2
% Additional	12.9
% Generous	1.7
% Disallowed	0.2

randomly selected by the program X-PLOR, the current model has an $R_{working}$ of 26.3% and R_{free} of 30.2% using reflections with an I/σ greater than 2.0 (78,217 reflections) and within the resolution range of 2.7–8.0 Å. The program PROCHECK[35] was used to calculate the refinement statistics summarized in Table 4.

MALDI experiments

BoGDH was dialyzed exhaustively against 0.1 M sodium phosphate (pH 7.0) buffer that contained 10 mM EDTA and adjusted to a final concentration of 1 mg/ml. The trypsin to GDH ratio (w/w) was adjusted to 1:100. Reaction volume was 21 μl, and 0.50 μl was removed from the reaction at 60 minutes, placed directly on the MALDI analysis plate, and allowed to dry before the addition of matrix 0.5 ml of 3,5-dimethoxy-4-hydroxy cinnamic acid (Aldrich) in a saturated solution of acetonitrile:water (50:50) 0.25% trifluoroacetic acid. On-plate digestions (data not shown) were performed at room temperature by using a mass spectrometer sample plate derivatized with trypsin (Intrinsic Bioprobes, Tempe, AZ). MALDI-MS mass analysis was conducted by using a Perceptive Biosystems (Framingham, MA) Voyager Elite equipped with delayed extraction and a nitrogen laser. Quantitative MALDI data was obtained using ACTH as an internal standard. External calibration typically was accurate to 0.05% and allowed unequivocal assignment of most proteolytic fragments. The identity of trypsin released fragments was determined by the Protein Analysis Worksheet (PAWS, MacIntosh version 6.0b2, copyright 1995, Dr Ronald Beavis) available on the Internet. MALDI-MS mass analysis was conducted by using a Perceptive Biosystems Voyager Elite and a Kratos Analytical Instruments MALDI-IV, both equipped with delayed extraction and nitrogen lasers.

Protein Data Bank accession number

The coordinates for this structure have been deposited to the Protein Data Bank and have been assigned the accession number of 1L1F.

This work was supported by grants from the National Institutes of Health (GM10704 and DK53012) to T.J.S. and C.A.S., respectivley, and from the American Diabetes Association to C.A.S. and T.J.S. (grant number 1320000170). The program MolView† was used to create all of the Figures.[30]

† http://www.danforthcenter.org/smith

References

1. Peterson, P. & Smith, T. J. (1999). The structure of bovine glutamate dehydrogenase provides insight into the mechanism of allostery. *Structure*, **7**, 769–782.
2. Smith, T. J., Peterson, P. E., Schmidt, T., Fang, J. & Stanley, C. (2001). Structures of bovine glutamate dehydrogenase complexes elucidate the mechanism of purine regulation. *J. Mol. Biol.* **307**, 707–720.
3. Frieden, C. (1965). Glutamate dehydrogenase VI. Survey of purine nucleotides and other effects on the enzyme from various sources. *J. Biol. Chem.* **240**, 2028–2037.
4. George, S. A. & Bell, J. E. (1980). Effects of adenosine 5′-diphosphate on bovine glutamate dehydrogenase: diethyl pyrocarbonate modification. *Biochemistry*, **19**, 6057–6061.
5. Bailey, J. S., Bell, E. T. & Bell, J. E. (1982). Regulation of bovine glutamate dehydrogenase. *J. Biol. Chem.* **257**, 5579–5583.
6. Iwatsubo, M. & Pantaloni, D. (1967). Regulation De L′ Activite′ De La glutamate dehydrogenase par les effecteurs GTP et ADP: ETUDE par "stopped flow". *Bull. Soc. Chem. Biol.* **49**, 1563–1572.
7. Koberstein, R. & Sund, H. (1973). The influence of ADP, GTP and L-glutamate on the binding of the reduced coenzyme to beef-liver glutamate dehydrogenase. *Eur. J. Biochem.* **36**, 545–552.
8. Dieter, H., Koberstein, R. & Sund, H. (1981). Studies of glutamate dehydrogenase. The interaction of ADP, GTP, and NADPH in complexes with glutamate dehydrogenase. *Eur. J. Biochem.* **115**, 217–226.
9. Fang, J., Macmullen, C., Smith, T. J. & Stanley, C. A. (2002). Expression, purification, and characterization of human glutamate dehydrogenase (GDH) regulatory mutations associated with a dominantly expressed congenital hyperinsulinism/hyperammonemia syndrome. *Biochem. J.* **363**, 81–87.
10. Frieden, C. (1959). Glutamic dehydrogenase. I. The effect of coenzyme on the sedimentation velocity and kinetic mechanism. *J. Biol. Chem.* **234**, 809–814.
11. Frieden, C. (1959). Glutamic dehydrogenase. II. The effect of various nucleotides on the association–disassociation and kinetic properties. *J. Biol. Chem.* **234**, 815–819.
12. Limuti, C. M. (1983). Glutamate dehydrogenase: equilibrium and kinetic studies. PhD thesis, University of Rochester.
13. Bayley, P. M. & O'Neill, T. J. (1980). The binding of oxidised coenzyme to bovine-liver glutamate dehydrogenase studied by circular-difference spectroscopy. *Eur. J. Biochem.* **112**, 521–531.
14. Dalziel, K. (1975). Kinetics and mechanisms of nicotinamide–nucleotide-linked dehydrogenases. In *The Enzymes* (Boyer, P. D., ed.), pp. 1–60, Academic Press, New York.
15. Bell, E. T., LiMuti, C., Renz, C. L. & Bell, J. E. (1985). Negative co-operativity in glutamate dehydrogenase. Involvement of the 2-position in the induction of conformational changes. *Biochem. J.* **225**, 209–217.
16. Weinzimer, S. A., Stanley, C. A., Berry, G. T., Yudkoff, M., Tuchman, M. & Thornton, P. S. (1997). A syndrome of congenital hyperinsulinism and hyperammonemia. *J. Pediatr.* **130**, 661–664.

17. Cheung, V. G., Gregg, J. P., Gogolin-Ewens, K. J., Bandong, J., Stanley, C. A., Baker, L. *et al.* (1998). Linkage-disequilibrium mapping without genotyping. *Nature Genet*, **18**, 225–230.
18. Kriwacki, R., Wu, J., Siuzdak, G. & Wright, P. (1996). Probing protein–protein interactions by mass spectrometry: analysis of the p21/Cdk2 complex. *J. Am. Chem. Soc.* **118**, 5320–5321.
19. Kriwacki, R., Wu, J., Tennant, L., Wright, P. & Siuzdak, G. (1997). Probing protein structure using biochemical and biophysical methods: proteolysis, MALDI mass analysis, HPLC, and gel-filtration chromatography of p21Waf1/Cip1/Sdi1. *J. Chromatogr.* **777**, 23–30.
20. Bothner, B., Dong, X. F., Bibbs, L., Johnson, J. E. & Siuzdak, G. (1998). Evidence of viral capsid dynamics using limited proteolysis and mass spectrometry. *J. Biol. Chem.* **273**, 673–676.
21. Kriwacki, R. & Siuzdak, G. (1998). Combined use of proteases and mass spectrometry in structural biology. *J. Biomol. Technol.* **9**, 5–15.
22. Bothner, B., Schneemann, A., Marshall, D., Reddy, V., Johnson, J. E. & Siuzdak, G. (1999). Crystallographically identical virus capsids display different properties in solution. *Nature Struct. Biol.* **6**, 114–116.
23. Thomas, J. J., Bakhtiar, R. & Siuzdak, G. (2000). Mass spectrometry in viral proteomics. *Acc. Chem. Res.* **33**, 179–187.
24. Broo, K., Wei, J., Marshall, D., Brown, F., Smith, T. J., Johnson, J. E. *et al.* (2001). Viral capsid mobility: a dynamic conduit for inactivation. *Proc. Natl Acad. Sci.* **98**, 2274–2277.
25. Stillman, T. J., Baker, P. J., Britton, K. L. & Rice, D. W. (1993). Conformational flexibility in glutamate dehydrogenase. Role of water in substrate recognition and catalysis. *J. Mol. Biol.* **234**, 1131–1139.
26. Peterson, P. E. & Smith, T. J. (1999). The structure of bovine glutamate dehydrogenase provides insights into the mechanism of allostery. *Structure*, **7**, 769–782.
27. Solovyev, V. V. & Salamov, A. A. (1991). Method of calculation of discrete secondary structures in globular proteins. *Mol. Biol.* **25**, 810–824.
28. Smith, T. J. & Bell, J. E. (1982). The mechanism of hysteresis in bovine glutamate dehydrogenase: the role of subunit interactions. *Biochemistry*, **21**.
29. Fisher, H. F. & Singh, N. (1991). Transduction of enzyme–ligand binding energy into catalytic driving force. *FEBS Letters*, **294**, 1–5.
30. Smith, T. J. (1995). MolView: a program to analyze and display atomic structures on the Macintosh personal computer. *J. Mol. Graph.* **13**, 122–125.
31. Otwinowski, Z. (1993). DENZO. In *Data Collection and Processing* (Sawyer, L., Isaacs, N. & Bailey, S., eds), pp. 56–62, SERC Daresbury Laboratory, Warrington, UK.
32. Otwinowski, Z. & Minor, W. (1997). Processing of X-ray diffraction data collected in oscillation mode. In *Methods in Enzymology* (Carter, C. W. J. & Sweet, R. M., eds), pp. 307–326, Academic Press, New York.
33. Baker, P. J., Britton, K. L., Engel, P. C., Farrantz, G. W., Lilley, K. S., Rice, D. W. & Stillman, T. J. (1992). Subunit assembly and active site location in the structure of glutamate dehydrogenase. *Proteins: Struct. Funct. Genet.* **12**, 75–86.
34. Brünger, A. T. (1992). *X-plor (Version 3.1) User's Guide*, Yale University, New Haven, CT.
35. Laskowski, R. A., MacArthur, M. W., Moss, D. S. & Thornton, J. M. (1993). PROCHECK: a program to check the sterochemical quality of protein structures. *J. Appl. Crystallog.* **26**, 283–291.

Edited by I. Wilson

(Received 14 December 2001; received in revised form 26 February 2002; accepted 27 February 2002)